Analysis of the Influence of Mine and Soil Properties on Features extracted from GPR Data

Friedrich Roth[a], Piet van Genderen[a], Michel Verhaegen[b*]

[a] Delft University of Technology, Faculty of Information Technology and Systems, International Research Centre for Telecommunications-transmission and Radar (IRCTR), Mekelweg 4, 2600 GA Delft, The Netherlands

[b] University of Twente, Faculty of Applied Physics, Systems and Control Engineering Division, Drienerlolaan 5, 7522 NB Enschede, The Netherlands

ABSTRACT

This paper presents a parametric study on the influence of target and soil properties, including depth of burial, on features extracted from ground penetrating radar (GPR) data. Understanding this influence is crucial for designing a classifier that uses these features for mine detection and identification. Two types of features have been studied. These are the Wigner-Ville distribution and geometric moments. Using a fast forward modeling program, synthetic GPR data were created for six buried objects, including two plastic minelike objects, for a wide range of soil properties and depths of burial. Both non-lossy and lossy soils were considered. From the computed data the above features were extracted and correlated with each other. The results show that the Wigner-Ville distribution performs much better in discriminating between objects than geometric moments. Furthermore, the features were found to be practically invariant to changes in mine-soil permittivity contrast and depth of burial provided that the soil is non-lossy. In the presence of losses, the GPR pulse is reshaped at the air-ground interface and as it propagates through the soil. As a result of the reshaping, the target response and hence the features can differ substantially from the non-lossy case.

Keywords: ground penetrating radar, landmine identification, Wigner-Ville distribution, geometric moments, soil properties, dispersion, discriminating power

1. INTRODUCTION

Recently, much research has been done on the identification of buried landmines based on features extracted from ground penetrating radar (GPR) data.[1,2,3] To achieve good classification performance, it is crucial to have accurate feature models for the targets in question. Due to the theoretical complexity of electromagnetic scattering from buried objects, feature values presumed to be characteristic for the targets are commonly determined experimentally at a controlled test site. However, the knowledge obtained like this only reflects the conditions at the test site and cannot be applied to other sites without caution. Constructing more generally valid feature models requires a thorough understanding of the information content of the features, i.e. the influence of target and soil properties, as well as depth of burial on the features needs to be understood.

Forward modeling has been shown to be a useful tool for studying the effect of target properties, soil type and depth of burial on the GPR response of buried objects.[4,5,6] In particular the effect on signal strength, crucial for detection, is well understood. However, the effect on features used for classification has hardly been addressed to date.

Using a ray-tracing program[7] specifically developed to model the GPR response to lossy, dispersive media, we studied the influence of the above factors on two types of features, namely the Wigner-Ville distribution[8] and geometric moments[9]. The analysis was divided into two parts. In the first part only non-lossy soils were considered. The second part of the analysis aimed at studying the influence of lossy soils, which are known to be associated with frequency dependence in both velocity and attenuation.[10,11]

* Further author information:
F.R.: E-mail: f.roth@its.tudelft.nl, Phone: +31/15/278 3815
P.v.G.: E-mail: p.vangenderen@its.tudelft.nl, Phone: +31/15/278 5055
M.V.: E-mail: m.verhaegen@tn.utwente.nl, Phone: +31/53/489 3181

For the non-lossy case, we considered six objects having different electrical properties and sizes, including two plastic minelike objects, all buried 5 cm deep. The effect of mine-soil permittivity contrast and depth of burial was examined for one of the minelike objects. In the second part of the analysis, we studied the effect of conduction losses, polarization losses, as well as their combined effect. In addition, we looked at the influence of depth of burial in lossy soil.

This paper is organized as follows. In section 2, a brief description of the modeling program is given and its assumptions and their implications on our study are discussed. In section 3, we review the definitions of the Wigner-Ville distribution and geometric moments, and explain how we have implemented them to extract features from an A-scan (Wigner-Ville distribution) and from a B-scan (geometric moments).[†] Examples of synthetic data for the non-lossy and lossy case are discussed in section 4 and 5 respectively. In addition, we present results from correlating the features extracted from the various data. A discussion of the discriminating power of the proposed features and their variance due to soil and depth variations follows in section 6.

2. DISPERSIVE GROUND PENETRATING RADAR MODELING

The GPR responses analyzed in this study have been computed using a 2.5 D modeling program developed by Powers[7]. The program is based on asymptotic ray theory and boundary element modeling in the frequency domain. An important characteristic of the program is that it computes a separate response for each significant frequency component of the starting pulse. Once all significant frequencies have been modeled, the time-domain response for each source-receiver position is obtained by Fourier Transformation of the respective cumulative frequency-domain response. This approach allows modeling the GPR response to lossy, dispersive media described by frequency dependent electrical and magnetic properties.

Each medium of the model is characterized by a conductivity, σ, and two sets of Cole-Cole parameters[12], defining the complex relative dielectric permittivity and the complex relative magnetic permeability respectively. The Cole-Cole parameters describe frequency dependence according to

$$\varepsilon_r = \varepsilon_r^{'} - \mathbf{i}\varepsilon_r^{''} = \varepsilon_\infty + \frac{\varepsilon_s - \varepsilon_\infty}{1 + (\mathbf{i}\omega\tau_\varepsilon)^{\alpha_\varepsilon}} \quad , \tag{1}$$

where ε_r is the relative dielectric permittivity consisting of a real part $\varepsilon_r^{'}$ and an imaginary part $\varepsilon_r^{''}$, ε_∞ is the real relative permittivity at infinitely high frequency, ε_s is the real relative permittivity at zero frequency, ω is angular frequency, τ_ε is the time constant of relaxation determined by the various polarization processes taking place, and α_ε is the time constant distribution parameter. An entirely similar equation can be written for the relative magnetic permeability. A frequency independent relative dielectric permittivity (magnetic permeability) can be realized by simply setting ε_∞ (μ_∞) equal to ε_s (μ_s). For all soils in our models we set $\mu_\infty = \mu_s = 1$, i.e. no ferromagnetic minerals are present. Detailed and very instructive explanations of the physical meaning of the Cole-Cole equation (1) are given by Olhoeft[10] and Powers[11].

The modeling algorithm is based on the following assumptions. First, the subsurface model is assumed to be infinite and horizontal in the dimension perpendicular to the acquisition line. Thus buried objects need to be modeled as infinitely long cylinders. The term 2.5 D modeling refers to the fact that the program accounts for both in-plane and out-of-plane geometrical spreading. As for the antenna system, it is assumed to be monostatic, consisting of a dipole antenna whose electric field axis is oriented perpendicular to the acquisition line. Consequently no polarization phenomena are considered. Furthermore, all reflecting interfaces are assumed to be in the far-field of the antenna. The far-field of an antenna for a given frequency can approximately be taken to begin at a distance of one wavelength from the antenna.[13] This far-field assumption needs to be adhered to in the model definition. We used a Ricker wavelet having a peak amplitude frequency of 1.5 GHz as a starting pulse. Hence, to meet the far-field assumption for most of the energy of the starting pulse, we chose an antenna height of 0.5 m above the air-ground interface for all our models.

The reason for choosing Powers' modeling program for this study was twofold. An important deciding factor was speed of computation. All B-scans shown in this paper were computed in less than 10 seconds on a Pentium II 400 MHz laptop computer. Therefore studying an object's GPR response as a function of soil properties and burial depth can be done in a reasonable amount of time. Second, as mentioned above the program allows modeling the effect of lossy, dispersive soils on the target response. In spite of these desirable attributes, it is important to note that ray methods are most accurate for smooth, continuous reflectors. Wave phenomena such as diffractions from corners are not produced. Hence, to ensure

[†] An A-scan refers to the time sampled return signal recorded at one source-receiver position. A B-scan is a set of A-scans recorded along a line.

relatively smooth reflecting surfaces, the minelike objects modeled in this study were given round edges. The shapes of all modeled objects are described in detail in section 4.

3. FEATURE EXTRACTION AND CROSS-CORRELATION

Before features were extracted, i.e. computing the Wigner-Ville distribution and the geometric moments, the reflection of the air-ground interface was removed from the data. This was achieved by simply averaging all A-scans of a B-scan and then subtracting this average scan from each A-scan. This technique is commonly used in GPR data processing. No additional preprocessing, such as gaining, was applied to enhance the data.

3.1. Wigner-Ville Distribution

For each modeled GPR response we computed the Wigner-Ville distribution of the A-scan corresponding to the antenna position right above the center of the buried object. The Wigner-Ville distribution of a discrete time signal $s(t_i)$ is given by[8]

$$W(t_i, f_j) = \frac{T}{\pi} \sum_{k=-\infty}^{\infty} s^*(t_i - kT)\, s(t_i + kT)\, e^{-i4\pi f_j kT} \quad , \tag{2}$$

where f is frequency, T is the time sampling interval and the superscript "*" denotes complex conjugate.

The Wigner-Ville distribution is a so-called time-frequency distribution. It fulfills the time and frequency marginals, i.e. integrating the Wigner-Ville distribution over all frequencies yields the instantaneous signal energy, $|s(t)|^2$, while integrating it over all times gives the energy density spectrum, $|S(f)|^2$, $S(f)$ being the Fourier Transform of the signal $s(t)$. Consequently integrating the Wigner-Ville distribution over all frequencies and all times yields the total signal energy. For these reasons, it is tempting to interpret the Wigner-Ville distribution as representing energy density as a function of time and frequency. However, there are two well-known properties of the Wigner-Ville distribution, which directly contradict this interpretation. First, the Wigner-Ville distribution is not manifestly positive for each time-frequency pair and second, its quadratic nature generally introduces energy artifacts in terms of cross-terms. Despite these deficiencies, the Wigner-Ville distribution finds wide application in signal recognition and classification.

Other than removing unwanted signal components before computing the Wigner-Ville distribution, a common way to reduce cross-term interference is to use the analytic signal associated with the actual signal.[8] The analytic signal is defined as having a real part equal to the actual signal and an imaginary part equal to the actual signal's Hilbert Transform. Taking the analytic signal removes the redundant negative part of the actual signal's spectrum, which would otherwise interfere with the positive frequencies. Accordingly, we used the analytic signal of the A-scan in the Wigner-Ville distribution computation.

3.2. Geometric Moments

Geometric moments have their origin in object identification for computer vision. They describe shapes and intensity distributions in images. The $(p+q)^{\text{th}}$ order geometric moment, denoted by m_{pq}, is defined as[9]

$$m_{pq} = \sum_{(i,j)\in\zeta} i^p\, j^q\, f(i, j), \qquad p, q = 0,1,2,3,... \tag{3}$$

where ζ is the image region of interest and $f(i, j)$ is the image intensity at the pixel with coordinates (i, j).[‡]

Viewing each time-position sample of a B-scan as an image pixel with intensity f and using a uniform temporal and spatial sampling from B-scan to B-scan, the theory of geometric moments can be applied to GPR data. Since B-scans do not consist of positive intensity values in the traditional image sense, but rather of positive and negative amplitude values, we considered two classes of geometric moments: one for which the sum was taken only over samples with positive amplitude and one for which only samples with negative amplitude were considered. In the latter case, the absolute amplitude values were used in the summing.

We computed geometric moments within a window of 81 by 81 samples (1.9 ns by 80 cm) covering the apex of the hyperbola corresponding to the target response as depicted in figure 1. The exact location of the window was estimated automatically by an iterative procedure, which finds the location for which the intensity centroid of the "object" within the

[‡] Note the analogy to moments of a two-dimensional probability density function.

window coincides with the window center. The intensity centroid is defined as the coordinate pair (m_{10}/m_{00} , m_{01}/m_{00}), where by way of exception all window samples are considered, yet still only absolute amplitude values are used in the summing. In order that the geometric moments are invariant with respect to translation of the target response in both time and position, the coordinate origin $(0,0)$ was taken to be the sample at the center of the window.

In image analysis it is not common to use very high order moments for they are more sensitive to image noise. Therefore, we limited ourselves to geometric moments with p and q values of up to 5, yielding a total of 72 geometric moments.

Geometric moments of different orders usually exhibit large dynamic range variations. Hence when constructing a feature vector from geometric moments, they need to be appropriately weighted to ensure that high order moments do not dominate over low order moments. We weighted the geometric moments according to

$$\mu_{pq} = \frac{m_{pq}}{\sum_{(i,j)\in\varsigma} |i|^p |j|^q} \quad . \qquad p,q = 0,1,2,3,... \tag{4}$$

3.3. Cross-Correlation

To compare the sets of geometric moments and the Wigner-Ville distributions obtained for the various buried objects, soil models and depths of burial, the cross-correlation was used. The cross-correlation of two vectors or matrices is a measure of how much they resemble each other.

Given two sets of geometric moments, their cross-correlation was computed using

$$c_{\mathrm{GM}} = \frac{\sum_{p,q} \left(\mu^{+}_{pq}\right)_{\mathbf{1}} \left(\mu^{+}_{pq}\right)_{\mathbf{2}} + \left(\mu^{-}_{pq}\right)_{\mathbf{1}} \left(\mu^{-}_{pq}\right)_{\mathbf{2}}}{\left\{\sum_{p,q} \left(\mu^{+}_{pq}\right)^2_{\mathbf{1}} + \left(\mu^{-}_{pq}\right)^2_{\mathbf{1}}\right\}^{1/2} \left\{\sum_{p,q} \left(\mu^{+}_{pq}\right)^2_{\mathbf{2}} + \left(\mu^{-}_{pq}\right)^2_{\mathbf{2}}\right\}^{1/2}} \quad , \tag{5}$$

where the superscripts "+" and "-" relate to the two classes of geometric moments discussed in section 3.2 and the bold subscript is used to distinguish between the two sets of geometric moments. The closer the cross-correlation c_{GM} is to one the more the two sets of geometric moments resemble each other. A value of one occurs when they only differ by a constant scaling factor.

The cross-correlation of two Wigner-Ville distributions was computed according to

$$c_{\mathrm{WVD}} = \max_{k} \left(\frac{\sum_{i,j} \mathrm{W}_{\mathbf{1}}(t_i, f_j)\, \mathrm{W}_{\mathbf{2}}(t_{i-k}, f_j)}{\left\{\sum_{i,j} \mathrm{W}^2_{\mathbf{1}}(t_i, f_j)\right\}^{1/2} \left\{\sum_{i,j} \mathrm{W}^2_{\mathbf{2}}(t_i, f_j)\right\}^{1/2}} \right) , \tag{6}$$

where k is a time shift index and the bold subscript is used to distinguish between the two distributions. Again, the closer the cross-correlation c_{WVD} is to one the more the two distributions resemble each other. Shifting the second distribution over the first and finding the maximum correlation provides that the cross-correlation of two identical but time shifted distributions still equates to one.

4. OBJECTS BURIED IN NON-LOSSY SOILS

The GPR responses of six different objects all buried 5 cm deep[§] in non-lossy soil were computed to study the general discriminating power of the Wigner-Ville distribution and geometric moments. The objects considered were two plastic minelike objects, two rounded stones and two metal spheres. The minelike objects were modeled as rectangles with round corners. The first minelike object was given a width of 7 cm and a height of 3 cm, representative of a PMA-1 mine.[14] The second minelike object has a width of 10 cm and a height of 4 cm, similar to a PMA-3 mine.[14] Both minelike objects were

[§] All depths of burial referred to in this paper are with respect to the top of the object.

given a relative dielectric permittivity of 2.8, a relative magnetic permeability of 1, and a zero conductivity, which are typical for plastics and explosives. The stones were modeled as ellipses, one having a major axis of 3.5 cm and a minor axis of 1.5 cm and the other having a major axis of 7 cm and a minor axis of 3 cm. Both stones were oriented with their major axis oriented horizontally. The stones were considered as being non-conductive and non-magnetic and were given a relative dielectric permittivity of 6, which is representative for common rock-forming minerals.[15] The metal spheres were modeled as circles having a radius of 2.5 cm and 5 cm respectively. Their perfectly reflecting behavior was modeled by choosing very high values for their conductivity, their relative dielectric permittivity and their relative magnetic permeability. The shapes and properties of the six objects are summarized in table 1. For the soil a relative dielectric permittivity of 4 and a zero conductivity were selected. These values are representative for dry sand.[16]

After the GPR responses for all objects had been obtained, the Wigner-Ville distribution and the geometric moments for each GPR response were computed according to the procedures described in section 3. Examples of the computed GPR responses and the Wigner-Ville distributions that go with them are shown in figures 2 through 5. The displayed A-scans are the ones for which the Wigner-Ville distribution was computed, i.e. they correspond to antenna positions right above the center of objects. Looking at the A-scans, it can be seen that the returns from the large minelike object (figure 3) and the large stone (figure 4) are made up of energy reflected from the top of the object and energy reflected from its bottom arriving at a later time. The A-scan of the small minelike object (figure 2) does not exhibit these two energy components due to the object's small height; the energy reflected from its top and that reflected from its bottom appear as one arrival. The A-scan of the small metal sphere (figure 5) consists of one strong single reflection from the top of the sphere in agreement with the fact that it is a perfect reflector. These differences in signal structure are also readily visible in the Wigner-Ville distributions. The late arrival of energy reflected from the bottom of the large minelike object and the large stone respectively is clearly marked by "negative energy" (black). Furthermore, it can be noted that the return from the large stone is reversed in polarity with respect to the returns of the minelike objects. This is a direct result of the large stone having a higher and the minelike objects having a lower dielectric permittivity than the soil in which they are immersed. The Wigner-Ville distribution however is not affected by signal polarity. This property follows directly from its definition (equation 2).

The visual differences of the Wigner-Ville distributions are also reflected in the correlation coefficients (table 2) obtained from correlating the distributions with each other. The Wigner-Ville distribution performs well in discriminating between the different objects with the exception of the pair of metal spheres. This is explained by the fact that they are both perfectly reflecting the radar pulse when it impinges upon them, resulting in a virtually identical A-scan.

Correlating the sets of geometric moments with each other yielded the cross-correlation coefficients listed in table 3. Geometric moments clearly exhibit a much lower discriminating power than the Wigner-Ville distribution. In particular the great resemblance between the moments obtained for the large stone and those obtained for the minelike objects is rather disturbing, considering the great differences evident in the corresponding B-scans.

Next, we studied the influence of mine-soil permittivity contrast. For this we computed GPR responses of the small minelike object buried 5 cm deep for soil relative dielectric permittivities of 9, 16, 25 and 36. Again the Wigner-Ville distribution and the geometric moments were computed for each of the responses. These were then correlated with the distribution and the geometric moments obtained previously for the small minelike object given a soil relative dielectric permittivity of 4. All cross-correlation coefficients were greater than 0.99. There are two reasons for this result. First, an increase in permittivity contrast solely results in stronger reflections occurring at later times according to the decrease in velocity. The structure of the reflected signals however is unchanged. And secondly, due to the small burial depth and the relatively large antenna height of 0.5 m, the opening angle of the hyperbola corresponding to the target response is primarily determined by the time it takes the wave to travel between the antenna and the air-ground interface. The decrease in angle due to an increase in soil dielectric permittivity is negligible.

Similar negligible effects can be expected from slightly varying the depth of an object buried in non-lossy soil. As for the case of an increase in permittivity contrast, signal structure remains unchanged and the change in opening angle of the response is negligible. This was verified by modeling the response of the small minelike object for various depths ranging from 2.5 cm to 10 cm given a soil relative dielectric permittivity of 4. The Wigner-Ville distributions and geometric moments computed from these responses were correlated with those obtained for a depth of 5 cm, yielding a minimum cross-correlation of 0.985.

5. INFLUENCE OF LOSSY SOILS

Losses in soils can be attributed to a variety of loss mechanisms.[10] When using GPR, losses are of concern not only with regard to signal strength but also because they introduce frequency dependence in velocity, attenuation, as well as transmission and reflection coefficients. As a result, the shape of a radar pulse changes as it propagates through the soil and when being reflected or transmitted at an interface.

In the following, we distinguish between conduction and polarization losses. Conduction losses are associated with charge transport phenomena, whereas polarization losses refer to the energy dissipation associated with polarization processes. In soils, conduction losses can predominantly be attributed to ionic conduction in water and polarization losses to the orientational polarization of water molecules. The overall strength of these losses is therefore directly related to water content. Dry soils are generally characterized by very low losses.

To study the effect of conduction losses, we modeled the GPR response of the large minelike object buried 5 cm deep in soil with a relative dielectric permittivity of 4 and a conductivity ranging from 10 mS/m up to 40 mS/m. Figure 6a displays the frequency dependence introduced by a non-zero conductivity. It can be seen that the frequency dependence is confined to frequencies below 500 MHz even for a conductivity of 40 mS/m. This was also reflected in the modeled GPR responses, which, apart from being weaker, showed great resemblance to the one computed for the non-lossy case ($\varepsilon_r = 4$, $\sigma = 0$ mS/m, depth of burial = 5 cm). The same was true for the Wigner-Ville distributions and geometric moments extracted from the data. Correlating the features with their non-lossy counterparts yielded cross-correlations no smaller than 0.993.

Modeling the effect of polarization losses resulted in more noticeable variations. Since polarization losses are associated with a frequency dependent complex dielectric permittivity as described by the Cole-Cole equation, we computed the GPR response of the large minelike object buried 5 cm deep for static real relative permittivities (ε_s) ranging from 9 up to 36. The other Cole-Cole parameters were fixed at $\varepsilon_\infty = 4$, $\tau_\varepsilon = 8$ ns and $\alpha_\varepsilon = 0.7$. These values roughly reflect the behavior of sandy soil for increasing water contents.[5,7] The conductivity was set equal to zero. Compared to conduction losses, polarization losses induce a much stronger frequency dependence in velocity, attenuation and ground surface transmission. This is shown in figure 6b. The attenuation in particular exhibits strong frequency dependence even at high frequencies (above 500 MHz). This frequency dependence greatly affects signal structure as illustrated in figure 7. As ε_s increases the energy arrivals from the top and the bottom of the large minelike object become indistinguishable. Results from correlating the features extracted from the computed data with their non-lossy counterparts are listed in table 4. As one might suspect, the cross-correlation coefficients decrease with increasing ε_s. It is interesting to note however that the decrease in cross-correlation observed for the geometric moments is much less than for the Wigner-Ville distribution.

Including both conduction and polarization losses in the soil model yielded slightly greater variations. Table 5 lists correlation coefficients obtained for the large minelike object buried 5 cm deep given various pairs of conductivity and static real relative permittivity. Again, the correlation was computed with respect to the object being buried 5 cm deep in non-lossy soil. As for the case of polarization losses only, feature deviation from the non-lossy case was much lower for geometric moments than for the Wigner-Ville distribution.

Finally, we returned to the case of varying depth of burial. The following parameters were chosen for the soil: $\varepsilon_s = 25$, $\varepsilon_\infty = 4$, $\tau_\varepsilon = 8$ ns, $\alpha_\varepsilon = 0.7$ and $\sigma = 30$ mS/m. We computed the GPR response of the large minelike object buried at depths ranging between 2.5 cm and 10 cm. In contrast to the non-lossy case, the Wigner-Ville distribution exhibited a strong dependence on burial depth. Correlating the Wigner-Ville distributions with the one obtained for the object being buried 5 cm deep in non-lossy soil yielded cross-correlation coefficients as low as 0.849 (depth of burial = 10 cm). The geometric moments on the other hand were more or less invariant to changes in depth of burial.

6. DISCUSSION

The modeling results demonstrate that the Wigner-Ville distribution is a useful feature set for object classification under many environmental conditions. Its ability to reveal local signal structure, such as the energy arrival from the bottom of an object, makes it more discriminating than geometric moments, which mainly embody global signal information. This characteristic of geometric moments directly follows from their definition, namely that they are sums of signal intensities. Hence one might say that fine discriminating information “drowns” in the overall information. A possible solution to this would be the use of a smaller computation window. When working with real data, a smaller window would also be required simply to ensure that it contains a minimum amount of clutter. It should be noted however, that a smaller computation window demands a more sophisticated approach to finding a well-defined window center than the one presented in this paper.

The effect of mine-soil permittivity contrast and depth of burial on the studied feature types has been shown to be negligible as a long as the soil is non-lossy. For lossy soils, such as wet soils, this is not necessarily the case. Losses are introduced by conductivity and energy dissipation associated with polarization processes. The polarization losses in particular can result in dispersion and a strongly frequency dependent attenuation over the operating band. The frequency dependence induced by conductivity is generally confined to the lower frequencies (below 500 MHz). In the presence of frequency dependent soil properties, the GPR pulse is reshaped at the air-ground interface and as it propagates through the soil. Energy arrivals from the top and the bottom of a dielectric object can become indistinguishable as the modeling showed for the large minelike object. As a result of the GPR pulse reshaping, the target response and extracted features differ from the non-lossy case. For the Wigner-Ville distribution, deviations from the non-lossy case of up to 0.849 as quantified by cross-correlation were observed. For geometric moments, the observed deviations were generally much lower, with a minimum observed cross-correlation of 0.977. Another modeling result is that for lossy soils feature deviation from the non-lossy case increases with depth of burial. This agrees with intuition. Summarizing, the Wigner-Ville distribution may be described as having a higher discriminating power than geometric moments but also as being more susceptible to frequency dependent soil properties.

With regard to object classification, frequency dependent soil properties can be a problem, especially when dealing with very wet soils. In the latter case one should be very careful in applying simple classifiers such as statistical classifiers. Taking another perspective, it might be argued that GPR mine identification is inherently spared from the worst frequency dependent soil effects by the very fact that high operating frequencies (above 500 MHz) are used. Generally frequency dependence is strongest at the lower frequencies. To avoid any misunderstandings, it should be added that the problem of signal detection, viewed independent of classification, becomes more difficult at high frequencies though due to attenuation. Another factor that reduces the impact of frequency dependent soil properties is the low burial depth of antipersonnel mines. It is worth noting that these two factors also in general justify the use of processing techniques that assume a stationary wavelet, i.e. the shape of the emitted pulse does not change as it propagates. These include migration and deconvolution.

Overall, it can be concluded that the chosen forward modeling approach leads to interesting, intuitively appealing results. The range of target and soil properties that we have considered in only a short period of time is beyond what could easily be realized experimentally. Yet, verification of the results based on real GPR data remains indispensable.

ACKNOWLEDGMENTS

This research was funded by the Dutch Technology Foundation STW, applied science division of NWO. The authors wish to thank Michael Powers from the U.S. Geological Survey for making his ray tracing software available to them.

REFERENCES

1. H. Brunzell, *Signal processing techniques for detection of buried landmines using ground penetrating radar*, PhD Thesis, Dept. of Signals and Systems, School of Electrical and Computer Engineering, Chalmers University of Technology, Göteborg, Sweden, 1998
2. D.R. Iskander, A.M. Zoubir, I. Chant, "Time-varying spectrum based detection of landmines using ground penetrating radar", in *Proc. of GPR 2000*, 8th Int'l. Conf. on Ground Penetrating Radar, May 23-26, 2000, Gold Coast, Australia, pp. 65-68, 2000
3. L. van Kempen, H. Sahli, E. Nyssen, J. Cornelis, "Signal processing and pattern recognition methods for radar AP mine detection and identification", in *IEE Conf. Publ. no. 458*, 2nd Int'l. Conf. on the Detection of Abandoned Landmines, Oct. 12-14, 1998, Edinburgh, UK, pp. 81-85, 1998
4. T.P. Montoya and G.S. Smith, "Land mine detection using a ground-penetrating radar based on resistively loaded vee dipoles", *IEEE Trans. Antennas Propagat.*, **47**, no.12, pp. 1795-1806, 1999
5. M.H. Powers, "Computer modeling to transfer GPR UXO detectability knowledge between sites", in *Proc. UXO Forum 1996*, March 26-29, 1996, Williamsburg, VA, USA, pp. 347-356, 1996
6. A. Sullivan, N. Geng, L. Carin, L. Nguyen, J. Sichina, "Performance analysis for radar detection of buried anti-tank and anti-personnel land mines", in *Proc. SPIE* **3710**, Detection and Remediation Technologies for Mines and Minelike Targets IV, April 5-9, 1999, Orlando, FL, USA, pp. 1043-150, 1999
7. M.H. Powers, *Dispersive Ground Penetrating Radar Modeling in 2D*, PhD Thesis, T-4820, Dept. of Geophysics, Colorado School of Mines, Golden, CO, USA, 1995
8. L. Cohen, "Time-Frequency Distributions – A Review", *Proc. of the IEEE*, **77**, no. 7, pp. 941-981, 1989
9. R. Mukundan and K.R. Ramakrishan, *Moment Functions in Image Analysis: Theory and Application*, World Scientific, Singapore, 1998

10. G.R. Olhoeft, "Electrical, magnetic, and geometric properties that determine ground penetrating radar performance", in *Proc. of GPR'98*, 7th Int'l. Conf. on Ground Penetrating Radar, May 27-30, 1998, The University of Kansas, Lawrence, KS, USA, pp. 177-182, 1998
11. M.H. Powers, "Modeling frequency-dependent GPR", *The Leading Edge*, **16**, no.11, pp. 1657-1662, 1997
12. K.S. Cole and R.S. Cole, "Dispersion and absorption in dielectrics, I, alternating current characteristics", *J. Chem. Phys.*, **9**, pp. 341-351, 1941
13. Y.T. Lo and S.W. Lee, *Antenna Handbook Vol. I: Antenna Fundamentals and Mathematical Techniques*, Van Nostrand Reinhold, New York, 1993
14. "Mine Identification Guide", *Humanitarian Demining Website*, www.demining.brtrc.com
15. G.V. Keller, "Rock and Mineral Properties", in *Electromagnetic Methods in Applied Geophysics Vol. 1: Theory*, M.N. Nabighian, ed., Soc. Explor. Geophys., Tulsa, OK, USA, 1987
16. A.P. Annan and S.W. Cosway, "Ground penetrating radar survey design", in *Proc. of SAGEEP'92*, Symposium for the Application of Geophysics to Engineering and Environmental Problems, April 26-29, 1992, Oakbrook, IL, USA, pp. 329-351, 1992

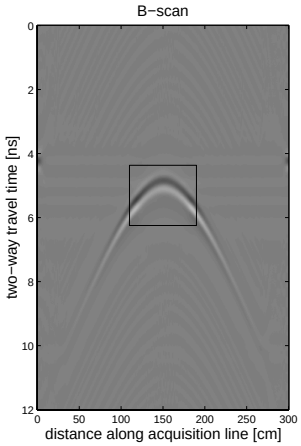

Figure 1: Geometric moments were computed within a window of 1.9 ns by 80 cm covering the apex of the hyperbola corresponding to the target response as illustrated here for the response of a metal sphere.

Table 1: Model parameters for the six objects.

	Shape	Dimensions	Rel. dielectric permittivity, ε_r	Rel. magnetic permeability, μ_r	Conductivity, σ [mS/m]
Small minelike object	rectangular	width: 7 cm height: 3 cm	2.8	1	0
Large minelike object	rectangular	width: 10 cm height: 4 cm	2.8	1	0
Small rounded stone	elliptical	major axis: 3.5 cm minor axis: 1.5 cm	6	1	0
Large rounded stone	elliptical	major axis: 7 cm minor axis: 3 cm	6	1	0
Small metal sphere	circular	radius: 2.5 cm	100	100	10000
Large metal sphere	circular	radius: 5 cm	100	100	10000

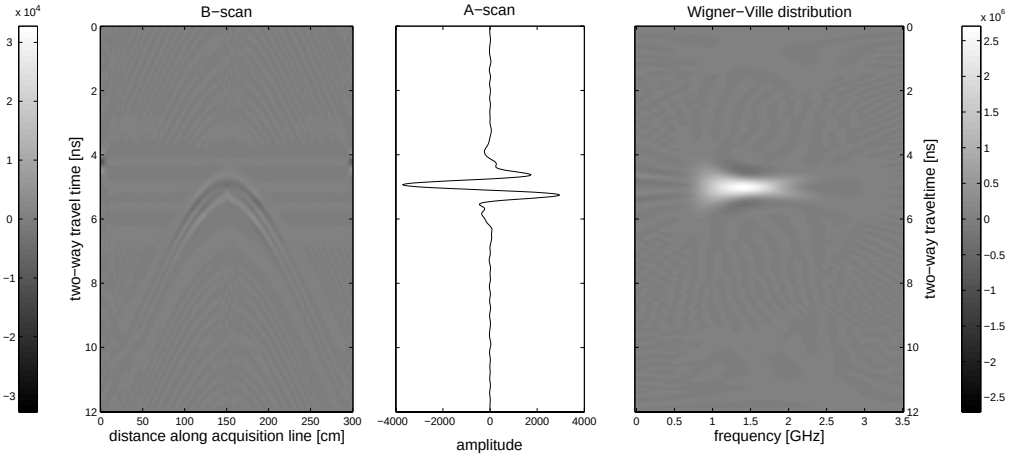

Figure 2: GPR response (after background subtraction) and Wigner-Ville distribution for the small minelike object buried in non-lossy soil ($\varepsilon_r = 4$, $\sigma = 0$ mS/m, depth of burial = 5 cm).

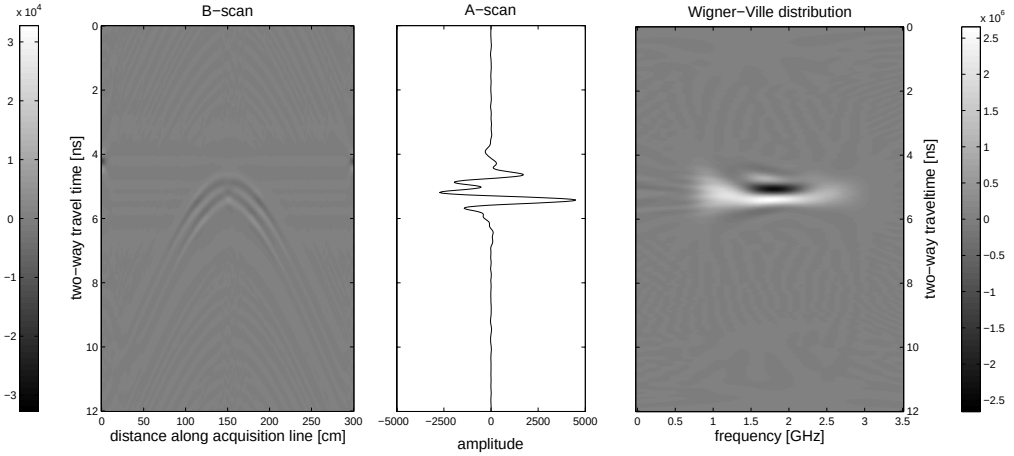

Figure 3: GPR response (after background subtraction) and Wigner-Ville distribution for the large minelike object buried in non-lossy soil ($\varepsilon_r = 4$, $\sigma = 0$ mS/m, depth of burial = 5 cm).

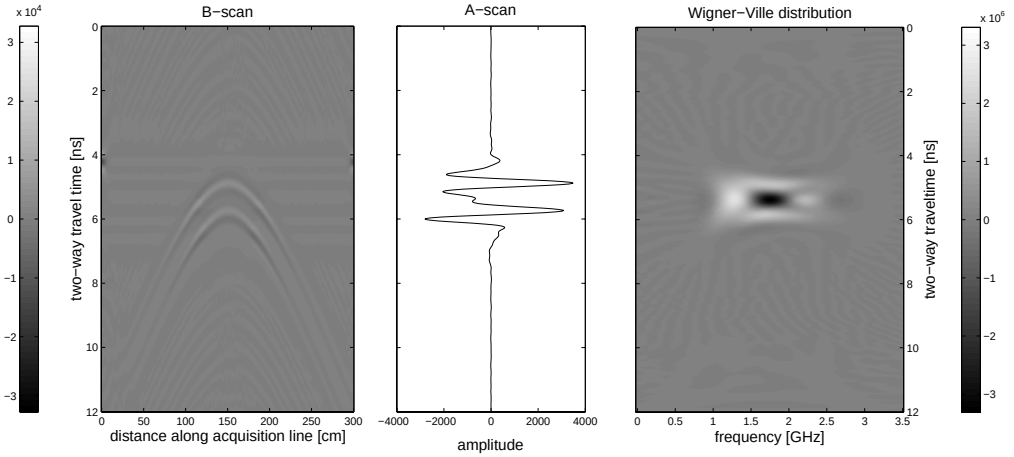

Figure 4: GPR response (after background subtraction) and Wigner-Ville distribution for the large stone buried in non-lossy soil ($\varepsilon_r = 4$, $\sigma = 0$ mS/m, depth of burial = 5 cm).

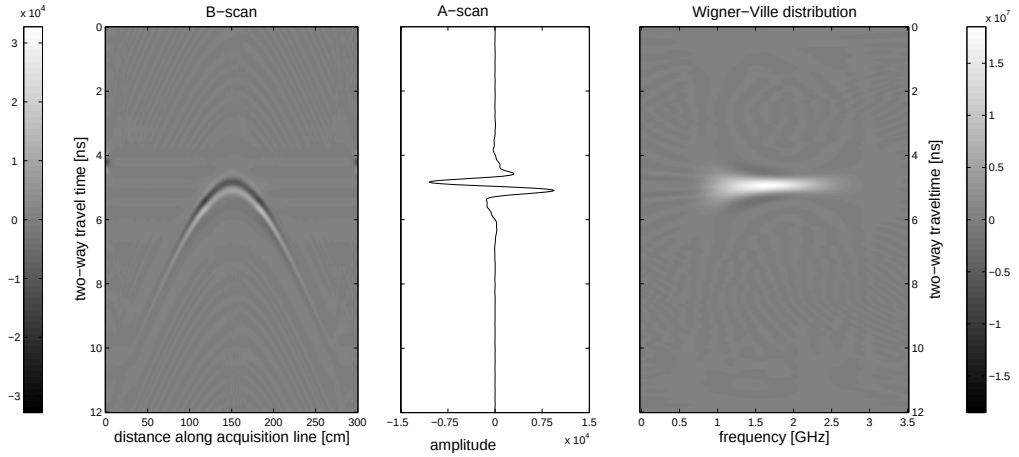

Figure 5: GPR response (after background subtraction) and Wigner-Ville distribution for the small metal sphere buried in non-lossy soil ($\varepsilon_r = 4$, $\sigma = 0$ mS/m, depth of burial = 5 cm).

Table 2: Cross-correlation coefficients (c_{WVD}) for the Wigner-Ville distributions associated with the six objects in non-lossy soil ($\varepsilon_r = 4$, $\sigma = 0$ mS/m, depth of burial = 5 cm).

	Small minelike object	Large minelike object	Small rounded stone	Large rounded stone	Small metal sphere	Large metal sphere
Small minelike object	1	0.707	0.474	0.488	0.9	0.901
Large minelike object		1	0.678	0.604	0.803	0.809
Small rounded stone			1	0.524	0.51	0.516
Large rounded stone				1	0.543	0.545
Small metal sphere					1	1
Large metal sphere						1

Table 3: Cross-correlation coefficients (c_{GM}) for the sets of geometric moments associated with the six objects in non-lossy soil ($\varepsilon_r = 4$, $\sigma = 0$ mS/m, depth of burial = 5 cm).

	Small minelike object	Large minelike object	Small rounded stone	Large rounded stone	Small metal sphere	Large metal sphere
Small minelike object	1	0.993	0.817	0.976	0.884	0.892
Large minelike object		1	0.859	0.982	0.912	0.918
Small rounded stone			1	0.881	0.951	0.947
Large rounded stone				1	0.902	0.906
Small metal sphere					1	0.999
Large metal sphere						1

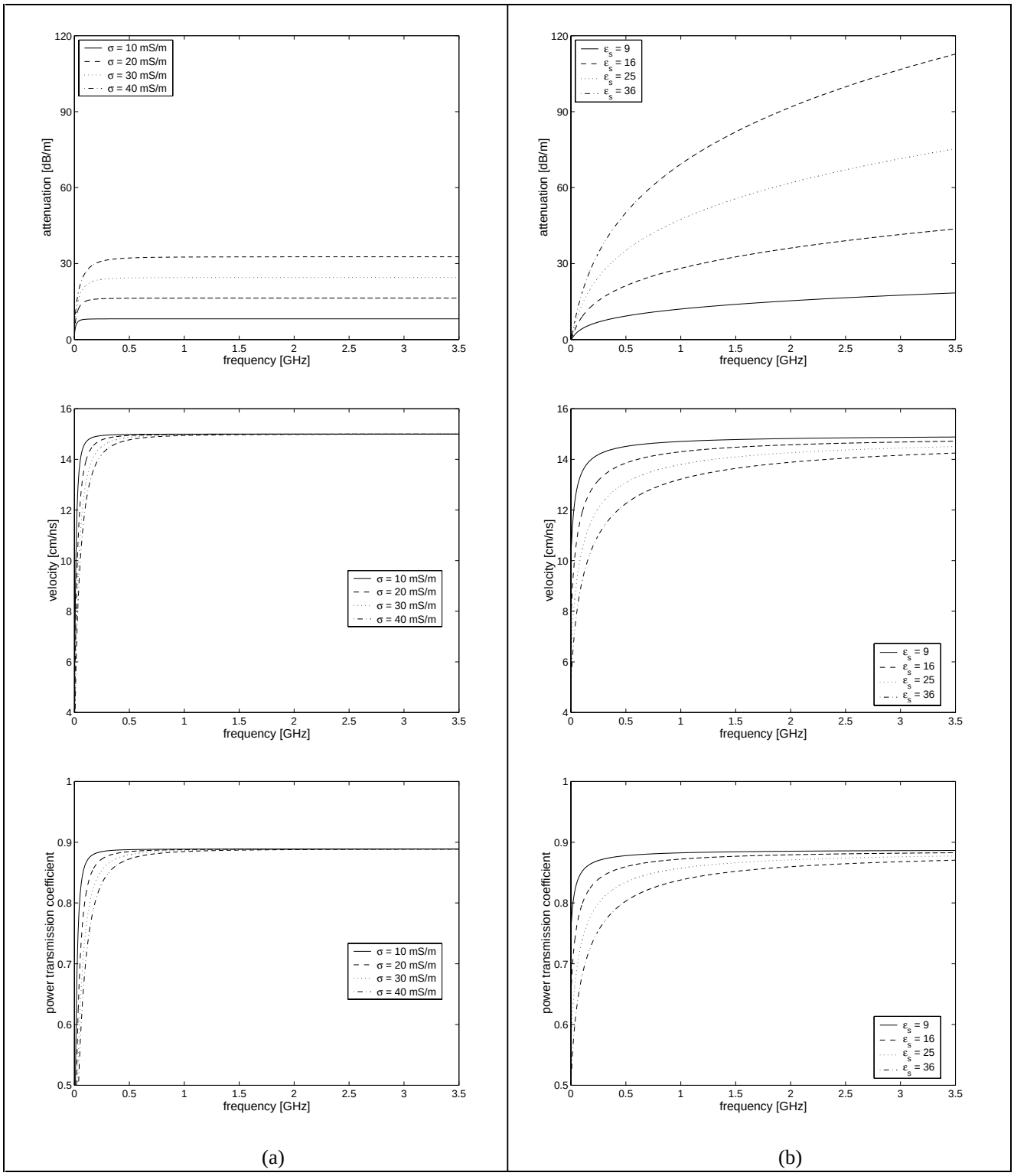

Figure 6: Attenuation, velocity and normal incidence power transmission coefficient of the air-ground interface as a function of frequency for (a) various soil conductivities with the soil relative dielectric permittivity fixed at $\varepsilon_r = 4$, and (b) various soil static real relative permittivities (ε_s) with the other soil properties fixed at $\varepsilon_\infty = 4$, $\tau_\varepsilon = 8$ ns, $\alpha_\varepsilon = 0.7$, $\sigma = 0$ mS/m.

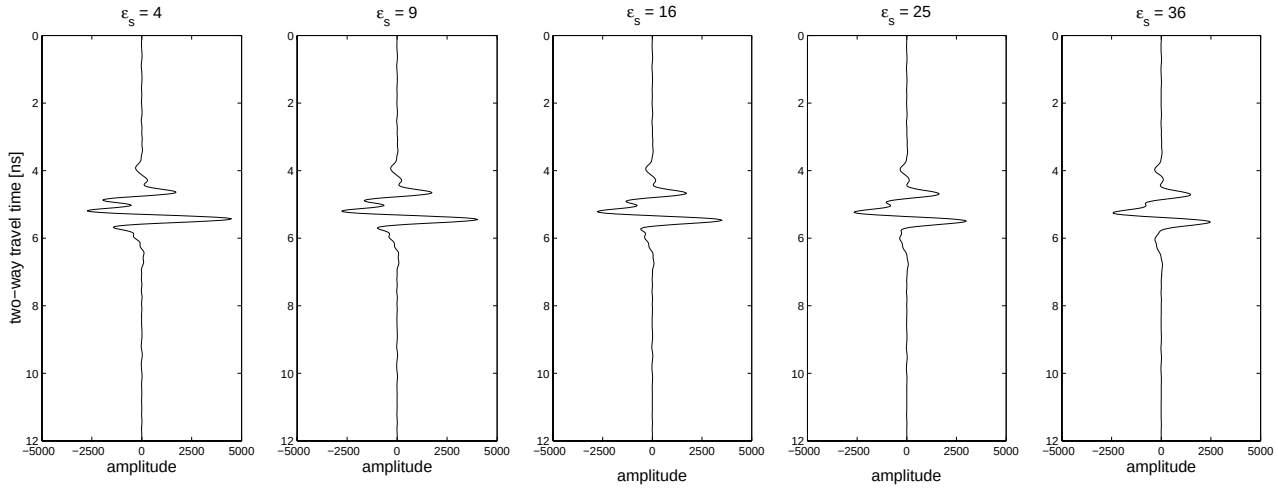

Figure 7: Change in pulse shape as a result of frequency dependent soil properties. Shown are A-scans (after background subtraction) of the large minelike object buried 5 cm deep for soil static real relative permittivities (ε_s) of 4, 9, 16, 25 and 36. The other soil properties were fixed at $\varepsilon_\infty = 4$, $\tau_\varepsilon = 8$ ns, $\alpha_\varepsilon = 0.7$, $\sigma = 0$ mS/m.

Table 4: Effect of polarization losses on the Wigner-Ville distribution and geometric moments of the large minelike object given a depth of burial of 5 cm. The cross-correlation coefficients are with respect to the object being buried in non-lossy soil ($\varepsilon_r = 4$, $\sigma = 0$ mS/m).

	$\varepsilon_s = 9$	$\varepsilon_s = 16$	$\varepsilon_s = 25$	$\varepsilon_s = 36$
c_{WVD}	0.997	0.985	0.96	0.925
c_{GM}	0.999	0.996	0.992	0.987

Table 5: Effect of conduction and polarization losses on the Wigner-Ville distribution and geometric moments of the large minelike object given a depth of burial of 5 cm. The cross-correlation coefficients are with respect to the object being buried in non-lossy soil ($\varepsilon_r = 4$, $\sigma = 0$ mS/m).

	$\sigma = 10$ mS/m $\varepsilon_s = 9$	$\sigma = 20$ mS/m $\varepsilon_s = 16$	$\sigma = 30$ mS/m $\varepsilon_s = 25$	$\sigma = 40$ mS/m $\varepsilon_s = 36$
c_{WVD}	0.994	0.974	0.943	0.901
c_{GM}	0.998	0.993	0.987	0.977